Metal−Semiconductor Zn−ZnO Core−Shell Nanobelts and Nanotubes

Xiang Yang Kong,[†,‡] Yong Ding,[‡] and Zhong Lin Wang*[,‡]

School of Materials Sciences and Engineering, Shanghai Jiao Tong University, Huashan Road 1954, Shanghai 200030, P.R. China, and School of Materials Science and Engineering, Georgia Institute of Technology, Atlanta, Georgia 30332-0245

Received: October 6, 2003

Heterostructured metal−semiconductor Zn−ZnO core−shell nanobelts and nanotubes have been synthesized. The core is a belt-shaped Zn single crystal, and the shell is an epitaxially grown ZnO layer of ~5 nm in thickness. The composite nanobelt grows along $[2\bar{1}\bar{1}0]$, its top/bottom being $\pm(0001)$, and side surfaces $\pm(01\bar{1}0)$. The Zn core is a single crystal, and the ZnO shell has an epitaxial orientation relationship with the core. The metal-based nanobelts have a distinct morphology from the nanowires reported in the literature. A growth mechanism is proposed on the basis of growth kinetics and thermodynamics. Sublimation of the Zn core results in the formation ZnO nanotubes.

Since the discovery of oxide semiconducting nanobelts,[1] one-dimensional (1-D) facet controlled nanomaterials have attracted much attention due to their potential applications in electronic and optoelectronic devices in nanoscale.[2] The terminology of "nanowires" is fairly popular in the literature, but nanowires represent quasi-one-dimensional nanomaterials that grow along a specific axial direction, whereas their side surfaces may not be well-defined. For nanobelts, it should be emphasized that they represent the 1-D nanomaterials that have specific growth direction and well-defined side facets. Analogous to carbon nanotubes, whose properties depend strongly on the helical angle at which the graphitic layer is rolled up, the properties of the nanowires and nanobelts should also depend on the anisotropic structure of their facet surfaces. Therefore, it is a critical step in materials synthesis to control the anisotropic growth of the side surfaces, which may lead to unique properties and selectivity.

Recently, a variety of quasi-one-dimensional ZnO nanomaterials have been synthesized, and they have been used for fabricating nanolasers,[3] field effect transistors[4] and gas sensors,[5] nanocantilevers,[6] and nanoresonators.[7] To enhance the multifunctionality, synthesis of 1-D nanocomposites is a direction. The coaxial nanocable of the SiC core and carbon sheath,[8] side-by-side silica−SiC nanowires,[9] metal silver nanowires sheathed with silica,[10] tape structured nanobelts of SnO_2 and TiO_2,[11] core−shell structured Si−Ge nanowires,[12] and ZnO−In_2O_3 core−shell nanostructure[13] have been synthesized. In this paper, we present a novel facet-controlled metal−semiconductor Zn−ZnO nanobelts, which are of rectangular cross-section and composed of metallic zinc core and semiconducting ZnO shell. The core and shell are single crystalline and they have an epitaxial orientation relationship. ZnO nanotubes are also found. A growth mechanism is proposed to understand the formation of the core−shell and tube structures. The metal−semiconductor epitaxially structured nanobelts could be useful for micro-electromechanical and nano-electromechanical systems.

The structurally controlled nanobelts were synthesized by a solid−vapor decomposition process.[1] Zn−ZnO core−shell nanbelts and nanotubes were synthesized with kinetic control in a solid−vapor phase deposition system. Pure ZnO powders were selected as source material, which was loaded in an alumina boat and positioned at the center of a horizontal tube furnace. The silicon substrates for collecting the products were positioned at the low-temperature region of the furnace. The synthesis process has two steps. The fist step is to control the evaporation and decomposition process, which was carried out by evacuating the alumina tube to $\sim 2 \times 10^{-3}$ Torr, raising the temperature to 1350 °C, and holding at the temperature for 5 min, but no carrier gas was introduced. The second step is to control the growth, which was also carried out at 1350 °C for 30 min but with the Ar carrier gas at a pressure of 200−250 Torr and flow rate of 25 sccm (standard cubic centimeters per minute). The substrate was placed downsteam in the temperature region 200−400 °C. Finally, the furnace was cooled slowly to room temperature.

The as-deposited products were characterized and analyzed by X-ray diffraction (Phillips PW 1800), scanning electron microscopy (SEM) (LEO 1530 FEG), transmission electron microscopy (TEM) (Hitachi HF-2000 FEG at 200 kV and JEOL 4000EX high-resolution TEM (HRTEM) at 400 kV), and energy-dispersive X-ray spectroscopy (EDS).

The sample was deposited on a silicon substrate, as shown by an optical image displayed in Figure 1a. The most interesting phenomenon is that the as-grown products are distributed at two distinct temperature regions, with the metallic luster in black being the Zn nanobelts and the white the ZnO nanobelts. Scanning electron microscopy (SEM) images show curly Zn nanobelts (Figure 1b) and straight ZnO nanobelts (Figure 1c). The Zn nanobelts were formed in a temperature rang of 200−300 °C, and they are distributed across a region of >4 cm in

* Corresponding author. E-mail: zhong.wang@mse.gatech.edu.
† Shanghai Jiao Tong University.
‡ Georgia Institute of Technology.

10.1021/jp036993f CCC: $27.50
Published on Web 12/02/2003

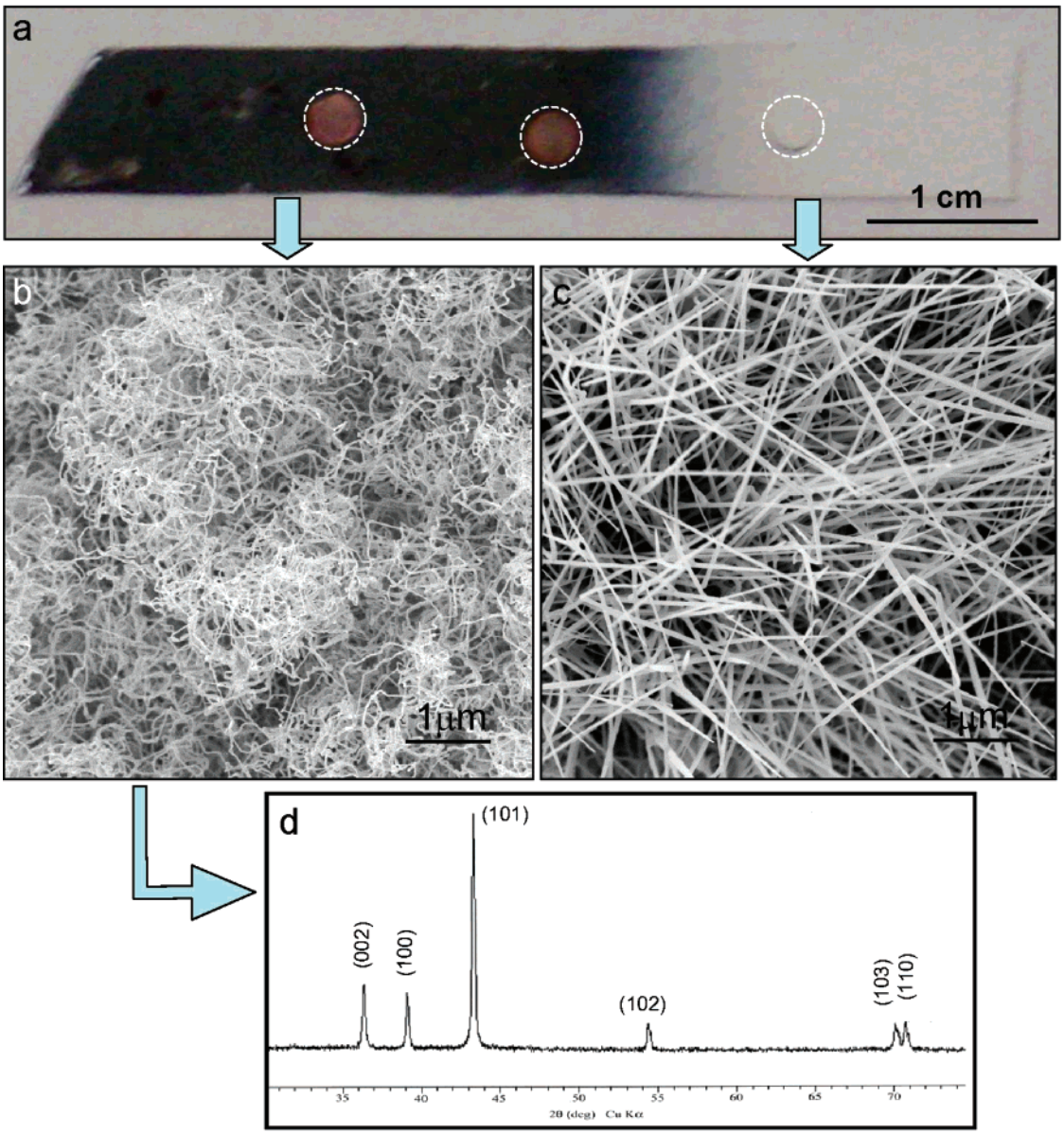

Figure 1. (a) Optical micrograph of the as-synthesized sample on a silicon substrate, showing two distinct products on the surface. The three circles indicate three TEM copper grids placed on the substrate for collecting samples. (b), (c) SEM images recorded from the metallic luster and white color regions, presenting the formation of pure Zn nanobelts and ZnO nanobelts, respectively. (d) XRD recorded from the metallic region, showing the formation of Zn nanobelts (The indexes were given on the basis of PDF No. 04-0831.)

length. The ZnO nanobelts were formed at a temperature range of 300−400 °C. The transition distance between the two different products is ∼0.5 cm. This apparently shows the structural control by growth temperature and kinetics.

The structure of the ZnO nanobelts has been investigated previously,[1] thus, this paper focuses on the Zn nanobelt collected from the metallic region. X-ray diffraction spectrum recorded from the metallic region indicates that the as-received product is dominated by zinc (Figure 1d). Transmission electron microscopy (TEM) images illustrate that the Zn nanobelts have widths of ∼50 nm (Figure 2a). Diffraction contrast across the structure suggests that it has a belt shape with a uniform thickness (the contrast presented in Figure 2a is due to the bending of the nanobelts along its length). Typical zigzag structures are frequently observed in the synthesized products. Dark-field image shows that the ZnO covering on the top and bottom (0001) surfaces is uniform in thickness, whereas the ZnO crystals on the side surfaces exhibit a grainy structure (Figure 2b), but the electron diffraction pattern (Figure 2c) recorded form the region indicates two sets of single-crystal diffraction spots, which are indexed to be [0001] Zn and [0001] ZnO with an epitaxial orientation. This type of composite nanobelt grows along $\langle 2\bar{1}\bar{1}0\rangle$, its top/bottom surfaces being $\pm(0001)$, and side surfaces $\{01\bar{1}0\}$. The zigzag structure presented in Figure 2b is due to a change in the growth direction from $[\bar{1}2\bar{1}0]$ to $[\bar{2}110]$, which are two crystallographically equivalent directions. A change in growth direction among the equivalent group of $\pm[2\bar{1}\bar{1}0]$, $\pm[1\bar{2}10]$, and $\pm[11\bar{2}0]$ produces turning points in the growth directions, resulting in the complex and curly shape of the nanobelts, as characterized by the TEM image (Figure 2a) and SEM image (Figure 1b). Energy-dispersive X-ray spec-

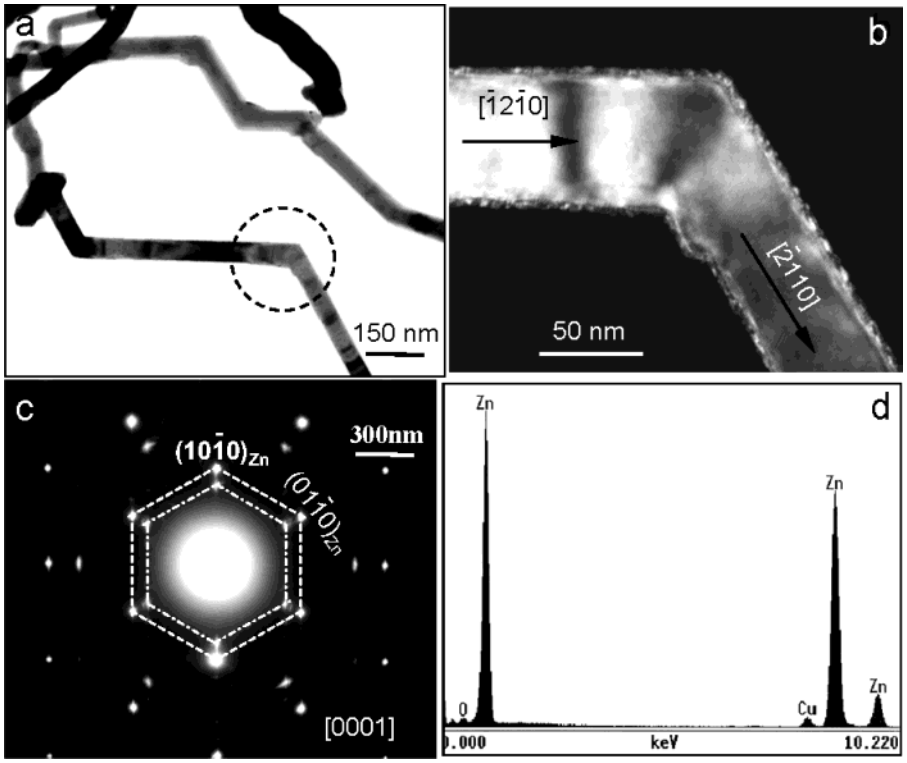

Figure 2. (a) Low-magnification TEM image of the as-synthesized Zn nanobelts with zigzag structure. (b) Dark-field TEM image from the circled region in (a), showing uniform contrast across its width and the surface ZnO layer. (c) Corresponding [0001] electron diffraction pattern recorded from the circled region in (a), displaying the presence of ZnO on the surface of the Zn nanobelt. (d) EDS spectrum recorded from the nanobelt, showing that the dominant element is Zn. The tiny Cu peak came from the TEM grid.

troscopy (EDS) shows that the nanobelt is dominated by Zn, with very little oxygen (Figure 2d).

The epitaxial Zn−ZnO nanobelt has been analyzed by high-resolution TEM (HRTEM). Figure 3a is a low-magnification TEM image of the nanobelt, displaying a Zn−ZnO core−shell structure. The most important point is that the shell has an epitaxial relationship with the core, as presented in the electron diffraction pattern, in which there are many weak reflection spots that were produced by double diffraction from the core and the shell. From the image and the diffraction pattern, it is apparent that the core is a single crystal and the shell is single crystalline, both having an epitaxial relationship with identical orientation. The diffraction pattern given in Figure 3 is equivalent to the one given in Figure 2c except there is a strong double diffraction effect, which is responsible for producing the extra reflection spots. Structurally, Zn and ZnO both have hexagonal crystal structure with lattice constants $a = 0.2665$, $c = 0.4947$ and $a = 0.3249$, $c = 0.5206$ nm,[14] respectively; thus, the mismatch between the two in $(10\bar{1}0)$ is ∼21.9% (in reference to Zn). The interference between the Bragg reflections from the two crystals produces Morie fringes in the image, which are apparent in the high-resolution TEM image presented in Figure 3b at the region where the Zn core and the ZnO shell overlaps. In the region there is only a ZnO shell, the HRTEM image shows clear lattice structure. The boundary between the Zn core and the ZnO shell is fairly sharp. Mismatch between the Zn core and ZnO shell produces defects and stacking faults at the interfacial region, which have been analyzed in detail and will be reported elsewhere.[15]

Nanotubes of ZnO have also been found in the metallic region. Parts a and b of Figure 4 show two typical TEM images of the ZnO nanotubes. The ZnO nanotubes may have a rectangular cross-section, the exterior surface of the tube is fairly uniform and smooth, whereas the inner surface is rough. Electron diffraction indicates that the nanotube has a single crystalline structure, but the TEM image shows that the nanotube is composed of nanocrystallites, all of which are oriented in the same orientation, so-called textured structure. The nanotube is along $[2\bar{1}\bar{1}0]$, its top/bottom surfaces being ±(0001). The HRTEM image given in Figure 4c shows the crystallized structure of the tube wall. In some cases, a tubular structure is found to be directly connected to a Zn−ZnO core−shell structure (Figure 4d). This gives a hint about the formation process of the tube.

Our synthesis experiment used ZnO powder as the raw material, whereas the produced products were Zn−ZnO core−shell nanobelts and ZnO nanobelts distributed in distinct temperature regions. It is well-known that the decomposition of ZnO occurs when it is subject to high enough temperature in a vacuum. The thermodynamics of these processes can be presented as the follows. The solid−vapor process and the decomposition process are expressed to be

$$\mathrm{ZnO(s)} \leftrightarrow \mathrm{ZnO(g)} \tag{1}$$

$$\mathrm{ZnO(g)} \leftrightarrow \mathrm{Zn(g)} + {}^{1}/_{2}\mathrm{O_2(g)} \tag{2}$$

The equilibrium constant function K_p for processes 1 and 2 as a function of temperature is given by[16]

$$-R \ln K_p(T) = \Delta H_{298}^{\circ}/T + \Delta G(T) \tag{3}$$

where ΔH is the change in free energy, $\Delta G(T)$ is the Gibbs

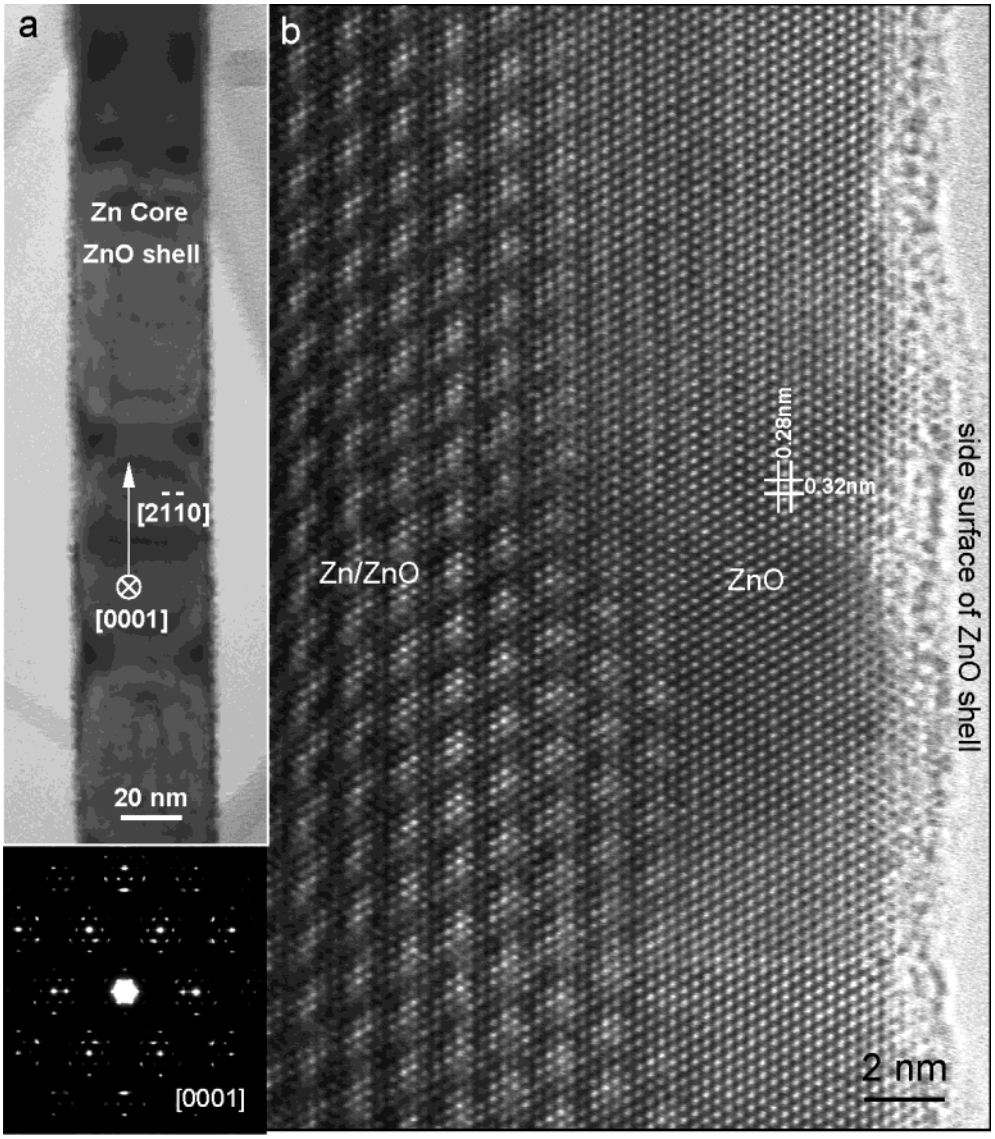

Figure 3. (a) Low-magnification TEM image of a Zn−ZnO core−shell heteronanobelt. (b) [0001] high-resolution TEM image recorded near the right-hand edge of a nanobelt, showing the Zn−ZnO overlap region and the ZnO wall. The corresponding electron diffraction pattern is given below (a).

energy, and $K_p = (P_{Zn(g)}P_{O_2}{}^{1/2})/P_e{}^{3/2}$, where P_{Zn} and P_{O_2} are the partial pressures of Zn and O_2, respectively, and P_e is the pressure in the growth chamber. Substituting the thermodynamic data into (3), one receives[16]

$$\ln(P_{Zn(g)}P_{O_2}{}^{1/2}/P_e{}^{3/2}) = -4.855 - 2474/T \qquad (4)$$

From eq 4, the saturation vapor pressure for Zn at 1350 °C is estimated to be $\sim 10^{-3}$ Torr, close to the preevacuated pressure in the growth chamber; hence, it is possible that part of the ZnO vapor decomposes into Zn vapor and O_2. Then, the ZnO vapor together with the Zn vapor are transported by Ar carrier gas to a lower temperature region, 200−400 °C (Figure 5a), which is cold enough to condense the vapor phase onto the substrate. The ZnO vapor condenses in the region 300−400 °C due to its higher sublimation temperature, resulting in the growth of ZnO nanobelts (the white region in Figure 1a); the Zn vapor condenses in the 200−300 °C region owing to lower sublimation temperature, resulting in the growth of Zn nanobelts, as shown in Figure 5b. The Zn nanobelt is dominated by a large (0001) facet due to its lowest surface energy.

On the other hand, the residual oxygen in the growth chamber as well as the oxygen decomposed originally from the raw material can oxidize the surface of the Zn nanobelts,[17,18] resulting in the formation of a thin ZnO shell on the surface. Because both Zn and ZnO have the hexagonal crystal structure, the ZnO shell tends to have an epitaxial orientation relationship with the Zn core, forming the Zn−ZnO core−shell nanobelts.

Moreover, Zn has a much lower melting point of 419 °C than that of 1975 °C for ZnO, it is possible for Zn to be sublimated out of the nanobelt in temperatures of 200−300 °C (see Figure 4d),[6] resulting in the formation of the ZnO nanotubes (Figure 5c). The exterior surface of the nanotube wall should be uniform and flat, as determined by the original geometry of the nanobelt, whereas the residual Zn on the inner surface of the wall could produce a roughness (see the image shown in Figure 4a).

In summary, this paper reports metal-based nanobelts that have a distinct morphology from the nanowires reported in the

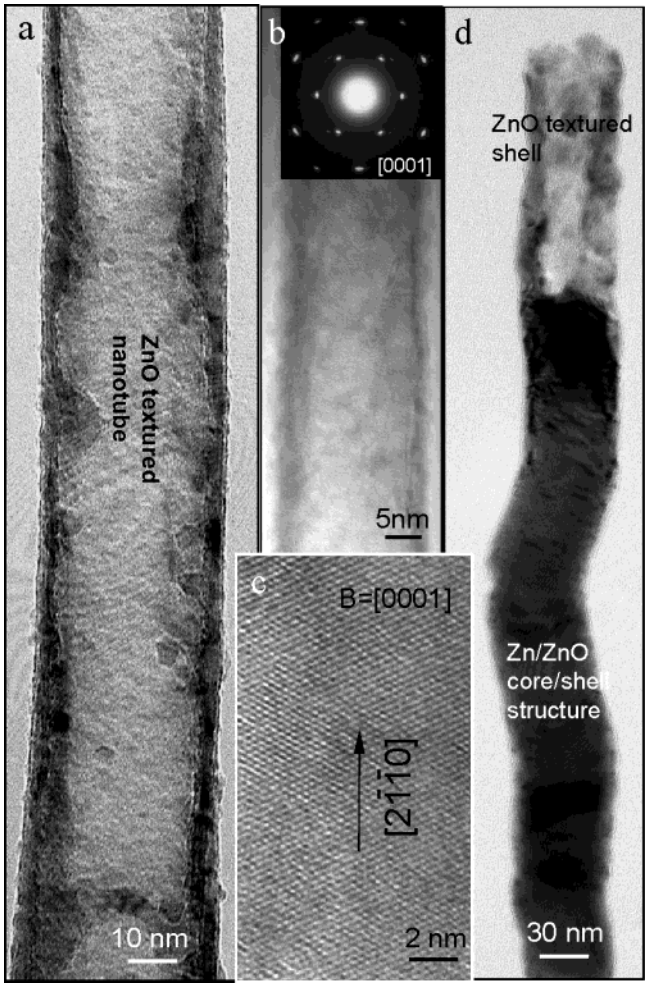

Figure 4. (a), (b) Low-magnification TEM imaged of the ZnO nanotubes. The sharp contrast for the nanotube in (a) is likely due to the sharp edge effect projected along its side surface, indicating that the nanotube may have a rectangular cross-section. The diffraction pattern inserted in (b) was recorded from the nanotube, presenting the textured structure of the ZnO nanocrystals composing the wall of the nanotube. The electron beam direction is [0001] and the tube grows along [2$\bar{1}\bar{1}$0]. (c) High-resolution TEM image recorded from the nanotube in (b), displaying the {01$\bar{1}$0} fringes. (d) TEM image of a short tube derived from a Zn−ZnO nanobelt. The contrast of the tube may indicates that part of the surface was fractured off during specimen preparation.

literature. Metal−semiconductor Zn−ZnO core−shell nanobelts and nanotubes have been synthesized by a solid−vapor process. The composite nanobelt grows along [2$\bar{1}\bar{1}$0], its top/bottom being ±(0001), and side surfaces ±(01$\bar{1}$0). The Zn core is a single crystal, and the ZnO shell has an epitaxial orientation relationship with the core. Sublimation of the Zn core results in the formation of ZnO nanotubes. The structures of the nanobelts and nanotubes have been characterized and a growth mechanism has been proposed on the basis of kinetics and thermodynamics. Heterostructured nanobelts could be tailored to exhibit superior functionality for various applications in nanotechnology, such as nanotransducers and nanosensors utilizing the unique facet controlled structure.

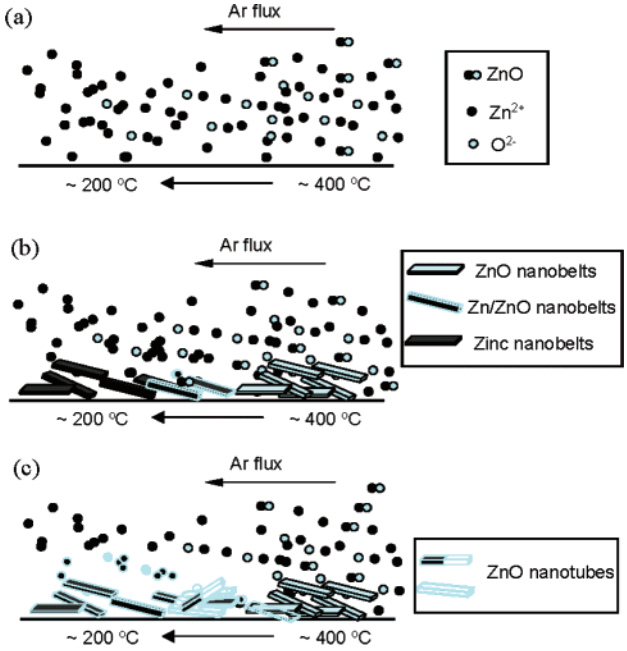

Figure 5. Proposed growth mechanism for the formation of the Zn−ZnO core−shell nanobelts and ZnO nanotubes. (a) ZnO, Zn, and O_2 vapor phases decomposed from pure ZnO raw materials at high temperature and carried by the Ar gas. (b) Deposition of the vapors at different substrate temperature regions resulting in the formation of ZnO nanobelts and Zn nanobelts, which subsequently transform into Zn−ZnO core−shell heteronanobelts after surface oxidation. (c) Vaporization/sublimation of the Zn core results in the formation of ZnO nanotubes.

References and Notes

(1) Pan, Z. W., Dai, Z. R. Wang, Z. L. *Science* **2001**, *291*, 1947.

(2) Wang Z. L., Ed. *Metals and Semiconductor Nanowires* and *Nanowires and Nanobelts of Semiconducting Materials*; Nanowires and Nanobelts; Kluwer Academic Publisher: New York, 2003; Vols. I and II.

(3) Huang, M. H.; Mao, S.; Feick, H.; Yan, H.; Wu, Y.; Kind, H.; Weber, E.; Russo, R.; Yang, P. *Science* **2001**, *292*, 1897.

(4) Arnold, M.; Avouris, P.; Pan Z. W.; Wang, Z. L. *J. Phys. Chem. B* **2003**, *107*, 659.

(5) Comini, E.; Faglia, G.; Sberveglieri, G.; Pan, Z. W.; Wang, Z. L. *Appl. Phys. Lett.* **2002**, *81*, 1869.

(6) Hughes, W. L.; Wang, Z. L. *Appl. Phys. Lett.* **2003**, *82*, 2886.

(7) Bai, X. D.; Wang, E. G.; Bai P. X.; Wang, Z. L. *Appl. Phys. Lett.* **2003**, *82*, 4806.

(8) Zhang, Y.; Suenaga, K.; Colliex, C.; Iijima, S. *Science* **1998**, *281*, 973.

(9) Wang, Z. L.; Dai, Z. R.; Gao, R. P.; Bai, Z. G.; Gole, J. L. *Appl. Phys. Lett.* **2000**, *77*, 3349.

(10) Yin, Y. D.; Lu, Y.; Sun, Y. G.; Xia, Y. N. *Nano Lett.* **2002**, *2*, 427.

(11) He, R. R.; Law, M.; Fan, R. Yang, P. *Nano Lett.* **2002**, *2*, 1109.

(12) Lauhon, L. J.; Gudiksen, M. S.; Wang, C. L.; Lieber, C. M. *Nature* **2002**, *420*, 57.

(13) Lao, J. Y.; Wen, J. G.; Ren, Z. F. *Nano Lett.* **2002**, *2*, 1287.

(14) Gallaso, F. *Structure and Properties of Inorganic Solids*; Pergamon Press: New York, 1970.

(15) Ding, Y.; Kong, X. Y.; Wang, Z. L. *J. Appl. Phys.*, in press.

(16) Hirschwald, W. *Z. Phys. Chem.* **1972**, *77*, 21.

(17) Hu, J. Q.; Li, Q.; Meng, X. M.; Lee, C. S.; Lee, S. T. *Chem. Mater* **2003**, *15*, 305.

(18) Wu, J. J.; Liu, S. C.; Wu, C. T.; Chen, K. H.; Chen, L. C. *Appl. Phys. Lett.* **2002**, *81*, 1312.